

CalibNet: Dual-branch Cross-modal Calibration for RGB-D Salient Instance Segmentation

Jialun Pei

CUHK

HKSAR, China

jialunpei@cuhk.edu.hk

Nian Liu

MBZUAI

Abu Dhabi, United Arab Emirates

liunian228@gmail.com

Tao Jiang

HUST

Wuhan, China

jtao99@hust.edu.cn

Yueming Jin

NUS

Singapore

ymjin@nus.edu.sg

He Tang

HUST

Wuhan, China

hetang@hust.edu.cn

Deng-Ping Fan*

ETH Zurich

Zürich, Switzerland

corresponding:dengpfan@gmail.com

Pheng-Ann Heng

CUHK

HKSAR, China

pheng@cse.cuhk.edu.hk

Abstract

We propose a novel approach for RGB-D salient instance segmentation using a dual-branch cross-modal feature calibration architecture called **CalibNet**. Our method simultaneously calibrates depth and RGB features in the kernel and mask branches to generate instance-aware kernels and mask features. **CalibNet** consists of three simple modules, a dynamic interactive kernel (DIK) and a weight-sharing fusion (WSF), which work together to generate effective instance-aware kernels and integrate cross-modal features. To improve the quality of depth features, we incorporate a depth similarity assessment (DSA) module prior to DIK and WSF. In addition, we further contribute a new **DSIS** dataset, which contains 1,940 images with elaborate instance-level annotations. Extensive experiments on three challenging benchmarks show that **CalibNet** yields a promising result, i.e., 58.0% AP with 320×480 input size on the COME15K-N test set, which significantly surpasses the alternative frameworks. Our code and dataset are available at: <https://github.com/PJLallen/CalibNet>.

1. Introduction

In recent years, depth maps have been introduced as an additional source of information to provide intuitive cues of spatial structure in the RGB-D Salient Object Detec-



Figure 1. Illustration of the RGB-D SIS task with the proposed CalibNet predictions. Our method propels RGB-D saliency detection to instance-level identification.

tion (SOD) task [30, 55]. While most RGB-D SOD approaches [21, 48, 56] have effectively utilized depth information by developing cross-modal feature fusion modules and depth quality assessment strategies in the backbone or decoder structure, relatively few approaches have incorporated depth awareness for instance-level saliency detection. However, salient instance segmentation (SIS) offers an opportunity to determine the location and number of each instance, which is particularly valuable for practical applications such as autonomous driving [5], video surveillance [15], and scene understanding [22]. Therefore, our work aims to take the first step towards incorporating depth-aware cues to enhance the RGB feature representation for RGB-D SIS (Fig. 1).

Currently, there are two popular frameworks (Fig. 2) that we can explore for introducing depth cues: the RPN-based framework (i.e., two-stage scheme) [13, 18] and the class&mask-based framework (i.e., one-stage) [7, 47]. De-

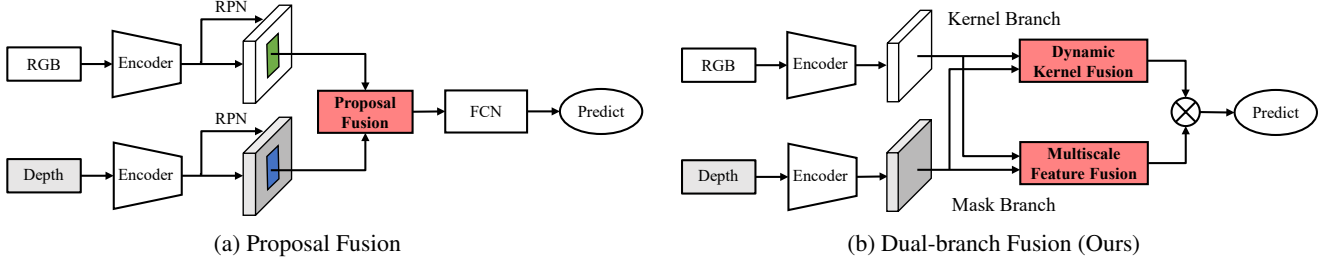


Figure 2. Comparison of two kinds of fusion architectures for RGB-D instance-level segmentation. (a) Proposal fusion in a two-stage manner [53]; (b) Our dual-branch fusion in a one-stage manner.

spite their great success, there are some important notes: i) Two-stage scheme requires additional proposal generation and refinement stages, which increases computational complexity and time. In addition, the generated proposals may not cover all instances or may result in false positives, leading to a decrease in performance. ii) For a one-stage framework, it may struggle with cases where depth and RGB information are inconsistent or noisy, potentially leading to inaccurate instance segmentation results.

Based on these observations, we have decided to design our approach based on the one-stage baseline, using a dual-branch cross-modal calibration scheme to fuse depth information in the *kernel* and *mask* branches. The approach comprises three key modules: 1) The Dynamic Interactive Kernel (**DIK**) module produces informative and structural attention maps using RGB and depth features. 2) The Weight-Sharing Fusion (**WSF**) module makes effective use of cross-modal mutual information and integrates shared features. 3) The Depth Similarity Assessment (**DSA**) module filters out noisy depth information and identifies valuable complements. Overall, our approach named **CalibNet**, aims to enhance the accuracy and reliability of the depth information used in the kernel and mask branches, resulting in more precise and robust segmentation results. Additionally, we utilize bipartite matching [3] to facilitate label assignment and reduce redundant predictions during inference, rather than relying on non-maximum suppression (NMS) post-processing. This enables us to achieve better segmentation performance while reducing computation overhead.

In addition, there are only two datasets available for RGB-D SIS task: COME15K [54] and SIP [12]. COME15K has the largest number of training samples but deficient annotation quality. SIP has highly accurate annotations, but only includes 929 images and focuses solely on the “person” category. To promote the development of RGB-D SIS and better evaluate model generalization performance, it is crucial to construct a moderately scale, high-quality annotated test set that includes multiple categories of salient instances. Thus, we contribute a new dataset, namely **DSIS**, which includes 1,940 images with detailed instance-level labels as well as depth maps. To better un-

derstand the development of existing SOTA techniques, we further evaluate CalibNet on three RGB-D SIS datasets, *i.e.*, COME15K, SIP, and our DSIS, making it the first systematic investigation in the RGB-D SIS field. Our main contributions include:

- To the best of our knowledge, **CalibNet** is the first basic framework for RGB-D SIS. The one-stage framework exploits depth information to optimize and interact with RGB features in the kernel and mask branches simultaneously, showing strong performance on all three RGB-D SIS datasets.
- Our new segmentation framework consists of three simple modules, which makes it easy to extend or introduce more complex components. The dynamic interactive kernel (DIK) module is included to highlight spatial and structural key locations and dynamically generate instance-level kernels. Additionally, the weight-sharing fusion (WSF) module improves the fusion efficiency of multiscale depth and RGB features in the mask branch. To calibrate the depth features, the depth similarity assessment (DSA) module excavates valuable depth information.
- We created a new dataset called **DSIS** to assess the generalization performance of RGB-D SIS models. Using DSIS and two existing datasets, we conducted the first large-scale RGB-D SIS study, evaluating 18 different baselines. We will make all benchmark results and tools publicly available to promote the development of instance-level saliency detection.

2. Related Work

Salient Instance Segmentation. Unlike the generic instance segmentation (GIS) task [8, 18, 47], SIS is class-agnostic because the identification of salient instances is based on the salient region, rather than specific class annotations. Li *et al.* [26] first proposed the SIS task and developed a multi-stage model, along with the first SIS dataset (ILSO). Since then, several SIS frameworks have been proposed, mostly based on the Mask R-CNN [18]. S4Net [13]

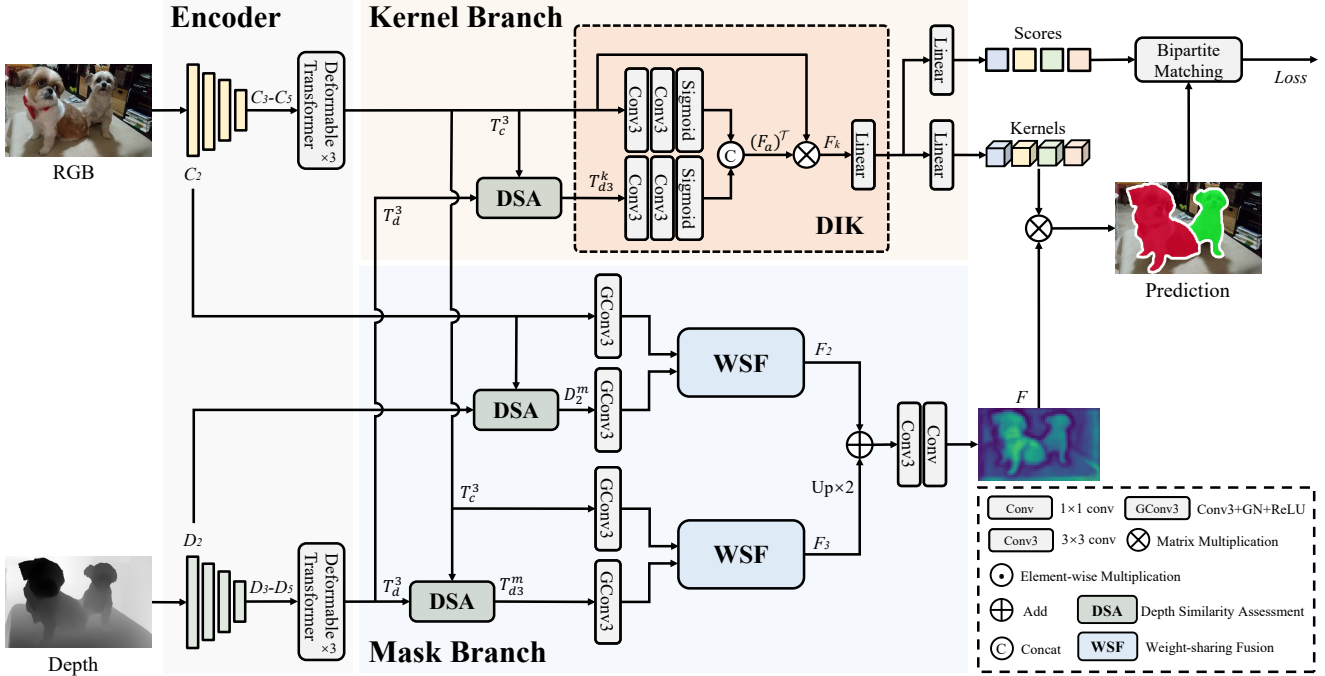


Figure 3. Detailed framework of the proposed CalibNet for RGB-D SIS. CalibNet consists of dual parallel branches: kernel and mask. In the kernel branch, the dynamic interactive kernel (DIK) module (Sec. 3.3) is designed to interact with RGB and depth features to generate instance-aware kernels; in the mask branch, our proposed weight-sharing fusion (WSF) (Sec. 3.4) identifies and calibrates cross-modal information at each level and then integrates multiscale low- and high-level features to achieve the mask feature. The depth similarity assessment (DSA) (Sec. 3.5) is embedded to evaluate the similarity of RGB and depth modal so as to calibrate the depth information.

introduced the first single-stage end-to-end framework for segmenting salient instances. On the basis of this, RDP-Net [51] adopted a regularized dense pyramid network to improve the feature pyramid and suppress non-informative regions. Similarly, SCG [31] added the saliency and contour branches in Mask R-CNN to enhance the recognition of salient instances. Unlike fully-supervised learning, Tian *et al.* [42] proposed a weakly-supervised network that adopts subitizing and class labels as weak supervision for SIS. More recently, OQTR [39] brought a transformer-based model that contains a cross-fusion module and salient queries to efficiently merge global features. Although these methods have led to the rapid development of the SIS task, they only focus on a single modality.

Instance Segmentation with RGB-D Data. While RGB-based instance segmentation models have made significant progress, instance segmentation with depth modality has been slower to develop. Earlier approaches, such as Gupta *et al.* [17] and Uhrig *et al.* [44], used multi-stage and fully convolutional networks, respectively. More recent methods, such as Xu *et al.* [53] and Xiang *et al.* [52], have used Mask R-CNN and synthetic data, respectively, to improve performance. To advance RGB-D instance-level segmentation further, we propose a novel RGB-D SIS framework that integrates depth features into both kernel and mask branches

based on the CNN-transformer encoder.

3. Proposed CalibNet

3.1. Overall Architecture

As shown in Fig. 3, the whole framework can be divided into four parts: (1) two individual encoders are adopted to extract multi-level RGB features and depth features respectively; (2) a depth similarity assessment module is applied to bridge the inherent disparity between appearance and structure information and purify the depth cues; (3) a kernel branch is introduced to interact with cross-modal features for producing instance-aware kernels; (4) a mask branch is designed to implicitly calibrate RGB and depth mutual information and fuse multiscale features to generate mask features.

3.2. Model Encoder

CalibNet extracts multi-level RGB features and depth modal features from two saliency encoders. For the RGB encoder, we first feed the input image I into the ResNet-50 [19] backbone to produce multiscale features denoted as $\{C_i | i=2, 3, 4, 5\}$. To enhance the global perception and provide higher-level features, a deformable transformer [57] is employed to further achieve global features ($\{T_c^i | i=3, 4, 5\}$)

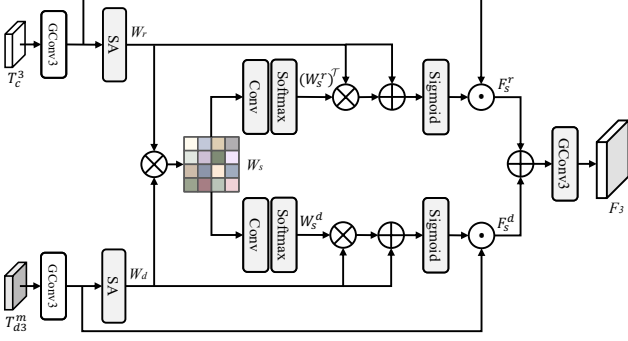


Figure 4. Structure of the proposed WSF module. The same operation is performed for the other scale (C_2, D_2^m). SA is the spatial attention (SA) [49] to generate spatial weights.

following the CNN architecture. Specifically, C_3 - C_5 are flattened and concatenated into a sequence that is used as the transformer input. To efficiently build the long-range dependencies, we adopt the vanilla deformable transformer encoder, which consists of a multi-head deformable self-attention module, layer normalization, and a feed-forward network (FFN). The RGB encoder stacks three deformable transformer layers sequentially and then restores the output sequence into the global features T_c^3 - T_c^5 .

For the depth stream, the CNN backbone has the same structure as the RGB encoder but without sharing weights. For convenience, the output features of the depth encoder are denoted as $\{D_i | i=2, 3, 4, 5\}$. Three deformable transformer layers are also embedded in the depth encoder to produce high-level depth feature representations, i.e., T_d^3 - T_d^5 . The multilevel feature maps output from the two modal encoders are fed into the kernel and mask branches for further interaction.

3.3. Kernel Branch

The kernel branch aims to integrate the RGB and depth features to discover distinctive cross-modal embeddings and generate a set of instance-aware kernels. To this end, we introduce a DIK module that exploits two modality-specific features to facilitate cross-modal interactions toward enhancing the granularity of instance-aware points. As illustrated in Fig. 3, the RGB feature $T_c^3 \in \mathbb{R}^{h \times w \times c}$ and the verified depth feature $T_{d3}^k \in \mathbb{R}^{h \times w \times c}$ after the DSA module (introduced in Sec. 3.5) are input to the DIK module. Here, h , w , and c refer to the height, width, and channel dimensions of the feature map. In the beginning, we concatenate two-channel fixed coordinates with T_c^3 and T_{d3}^k to preserve spatial locations in accordance with [32]. Bilaterally, the two modal features are operated by two successive 3×3 convolutional layers. In the latter instance-aware convolution, the dimension c of the two modal features is decreased from 256 to the number of salient kernels N in order to prioritize diverse potentially instance-aware embeddings.

Then, a sigmoid function and a concatenation operation are added to generate a cross-modal instance-aware attention map $F_a \in \mathbb{R}^{h \times w \times N}$. This process can be formulated as

$$F_a = \text{Cat}[\mathcal{S}(\mathcal{C}_3(\mathcal{C}_3(T_c^3))); \mathcal{S}(\mathcal{C}_3(\mathcal{C}_3(T_{d3}^k)))], \quad (1)$$

where \mathcal{S} represents the sigmoid function, \mathcal{C}_3 is a 3×3 convolution, and $\text{Cat}[\cdot]$ is the concatenation operation. According to the guidance of the attention map, $F_a \in \mathbb{R}^{h \times w \times N}$ can be viewed as the key value that is used to perform matrix multiplication with the RGB feature $T_c^3 \in \mathbb{R}^{h \times w \times c}$ to obtain instance-aware embeddings $F_k \in \mathbb{R}^{N \times c}$. This operation is described as

$$F_k = (F_a)^T \otimes T_c^3, \quad (2)$$

where \otimes denotes matrix multiplication and $(\cdot)^T$ is the transpose operation. Unlike using the cross-attention operation [3, 7] to obtain kernels, our DIK module is more lightweight that boasts adaptability to diverse multi-modal input settings. Finally, two linear layers are applied to achieve N instance-aware kernels. Besides, we also attain a set of confidence scores to suppress negative predictions.

3.4. Mask Branch

In tandem with the kernel branch, the mask branch is brought out to discover and calibrate distinctive information from cross-modal cues and fuse multiscale low- and high-level features, ultimately yielding a shared mask feature. For the input of the mask branch, we employ the low-level feature C_2 from the CNN backbone and the high-level feature T_c^3 from the deformable transformer in the RGB encoder to provide a rich appearance feature representation. In concurrence with C_2 and T_c^3 , depth features D_2 and T_d^3 from the depth encoder are also applied to enhance structural information and maintain the internal consistency of salient regions. We divide different modality features of the same scale into the same group (i.e., $\{C_2, D_2\}$, $\{T_c^3, T_d^3\}$). The details of the mask branch are described at the bottom of Fig. 3. Similar to the kernel branch, the input depth features D_2 and T_d^3 are also passed through the DSA module to obtain purified depth features D_2^m and T_{d3}^m . After a sequential operation (3×3 convolution, group normalization, and a ReLU function), the RGB and depth features are fed into the proposed WSF, which is designed to efficiently exploit complementary cross-modal features at different levels for a shared representation.

As illustrated in Fig. 4, the WSF module aims to implicitly calibrate and integrate cross-modal features based on a shared affinity weight which establishes strong correlations and reveals mutual information between the two modalities. Toward this goal, the two modal features first pass through a spatial attention (SA) [49] to produce individual spatial attention weights $W_r \in \mathbb{R}^{h \times w}$ and $W_d \in \mathbb{R}^{h \times w}$. Given the

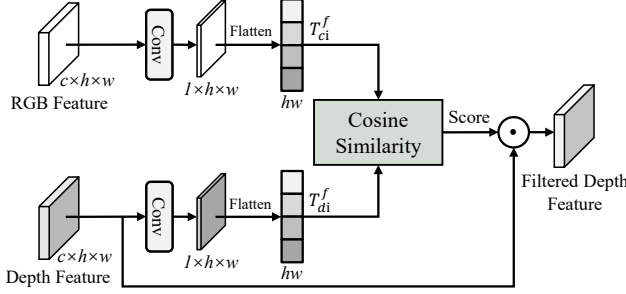


Figure 5. Diagram of the proposed DSA module.

depth feature T_{d3}^m , the process of SA can be described as

$$W_d = \mathcal{S}(\mathcal{C}_7(\text{Cat}[\mathcal{A}(T_{d3}^m); \mathcal{M}(T_{d3}^m)])), \quad (3)$$

where \mathcal{A} denotes the average-pooling operation and \mathcal{M} is the max-pooling operation. Consistently, D_2^m , C_2 , and T_c^3 pass through the same operation to obtain corresponding spatial attention weights. For better aggregation and calibration of cross-modal features, the shared affinity weight $W_s \in \mathbb{R}^{h \times h}$ is generated from the spatial weight maps W_r and W_d , which is calculated as

$$W_s = W_r \otimes (W_d)^\top. \quad (4)$$

It is worth noting that the shared affinity matrix W_s has a small size of $h \times h$, which avoids computing the pixel-to-pixel affinity weights ($hw \times hw$) [9, 29, 46]. Moreover, the affinity weight with a smaller size can greatly decrease the computational cost of subsequent operations in WSF (see Sec. 4.5). Once receiving the affinity weight W_s , we can generate the modality-specific weights $W_s^r \in \mathbb{R}^{h \times h}$ and $W_s^d \in \mathbb{R}^{h \times h}$ using two 1×1 convolution layers and the softmax function. Afterward, W_s^r and W_s^d are integrated with the previous spatial weights W_r and W_d by the matrix multiplication with the residual operation to enhance the modality-specific spatial attention and preserve the original modal features. An element-wise multiplication is followed to achieve the re-weighted RGB feature F_s^r and depth feature F_s^d . For instance, given the input features T_c^3 and T_{d3}^m , the two modal re-weighted features can be achieved as

$$\begin{cases} F_s^r = \mathcal{G}_3(T_c^3) \odot \mathcal{S}(W_r + (W_s^r)^\top \otimes W_r) \\ F_s^d = \mathcal{G}_3(T_{d3}^m) \odot \mathcal{S}(W_d + W_s^d \otimes W_d) \end{cases} \quad (5)$$

where \odot is element-wise multiplication, \mathcal{G}_3 denotes a sequential operation that contains a 3×3 convolution followed by group normalization, and a ReLU function. In this way, we can add re-weighted RGB and depth features (F_s^r and F_s^d) to obtain the fused cross-modal feature map F_3 with a scale of $1/8$. Similarly, we can also take C_2 and D_2^m as inputs and use WSF to obtain a finer fused feature F_2 with a scale of $1/4$.

Integrating the fused features across different scales is essential to generate a shared mask feature. In this regard, we concisely upsample F_3 to the $1/4$ scale and add it to F_2 . A 3×3 convolution followed by a 1×1 convolution is applied to produce the unified mask feature F . Finally, the instance-aware kernels and the mask feature are fed into the dynamic convolution operation to output salient instances.

3.5. DSA Module

As is well known, structural information and salient cues are not strongly correlated. Low-quality depth maps contain noisy information that interferes with the prediction of salient instances. For this purpose, we propose a DSA module that develops a similarity score by evaluating the correlation between RGB and depth information to adaptively weigh the depth features. In CalibNet, the DSA module is embedded before the kernel branch and the mask branch to calibrate the depth features. The diagram of our DSA module is shown in Fig. 5. Symmetrically, two modal features from the encoder pass through a 1×1 convolution to generate an attention map, respectively. Then, the RGB and depth attention maps are flattened to calculate their attention similarity. Notably, we adopt the cosine distance to calculate the similarity score due to its high sensitivity to directional and spatial considerations. Giving the flattened attention maps T_{ci}^f and T_{di}^f , the similarity score V_s is computed as

$$V_s = 1 - (1 - \frac{T_{di}^f \odot T_{ci}^f}{\|T_{di}^f\| \|T_{ci}^f\|})/2. \quad (6)$$

The range of the similarity score V_s is $[0, 1]$. The higher the value of V_s , the stronger the consistency of different modal features. Finally, we multiply the similarity score with the input depth features to optimize the fusion proportion of depth information.

3.6. Loss Function

For end-to-end training, the proposed CalibNet employs bipartite matching to assign confidence scores and instance masks. In line with DETR [3], we apply the Hungarian algorithm to optimize the paired matching between ground truths and predictions.

The training loss function is defined as follows:

$$\mathcal{L} = \lambda_c \mathcal{L}_c + \lambda_{mask} \mathcal{L}_{mask} + \lambda_{obj} \mathcal{L}_{obj} + \lambda_{bin} \mathcal{L}_{bin}, \quad (7)$$

where \mathcal{L}_c is the saliency localization loss that leverages the confidence score to determine salient instances. Specifically, focal loss [28] is used in \mathcal{L}_c . \mathcal{L}_{mask} is the segmentation mask loss combining Dice loss [35] and pixel-wise binary cross-entropy loss. Inspired by [8], we also embed the binary cross-entropy loss \mathcal{L}_{obj} for the IoU-aware objectness. In addition, we employ the auxiliary loss \mathcal{L}_{bin} to

Task	Method	Volume	COME15K-N [54]			COME15K-D [54]			DSIS			SIP [12]		
			AP	AP ₅₀	AP ₇₀	AP	AP ₅₀	AP ₇₀	AP	AP ₅₀	AP ₇₀	AP	AP ₅₀	AP ₇₀
SIS	S4Net [13]	CVPR19	43.7	68.0	52.5	37.1	60.9	43.2	58.3	81.9	71.8	49.6	76.0	63.7
	RDPNet [51]	TIP21	49.8	72.2	59.5	42.1	65.2	49.7	66.1	87.2	80.1	59.0	80.1	74.1
	OQTR [39]	TMM22	48.7	71.1	58.3	42.7	65.9	50.5	63.1	85.9	77.0	59.9	83.1	76.3
CIS	OSFormer [38]	ECCV22	53.0	71.9	61.3	45.8	66.3	52.4	67.9	86.3	78.3	63.2	80.5	74.6
GIS	Mask R-CNN [18]	ICCV17	48.8	71.2	58.6	42.2	65.7	50.8	65.6	86.8	80.2	57.9	79.8	73.3
	MS R-CNN [20]	CVPR19	49.7	70.4	58.9	42.3	63.8	50.0	66.8	87.3	80.3	60.0	79.8	73.3
	Cascade R-CNN [2]	TPAMI19	49.4	69.8	58.7	41.9	64.3	49.8	66.4	87.3	79.9	59.1	79.1	73.6
	CenterMask [25]	CVPR20	49.6	71.6	59.0	42.5	65.2	51.0	65.7	87.6	79.7	57.6	79.8	72.3
	HTC [6]	CVPR19	51.4	73.7	61.0	44.1	68.0	52.1	67.5	87.6	81.1	60.0	81.4	74.9
	YOLACT [1]	ICCV19	48.1	70.7	56.2	41.4	66.0	48.5	62.4	84.1	73.3	62.0	82.3	74.7
	BlendMask [4]	CVPR20	48.1	70.6	56.9	41.0	64.8	48.5	65.5	86.9	78.0	55.5	77.3	69.7
	CondInst [43]	ECCV20	49.6	72.0	59.5	42.8	66.4	51.0	65.1	86.8	79.1	58.6	79.4	73.3
	SOLOv2 [47]	TPAMI21	51.1	71.6	59.9	45.1	66.3	52.8	67.4	87.0	80.4	63.4	80.7	74.8
	QueryInst [14]	CVPR21	51.5	73.1	61.1	43.9	67.5	51.8	67.9	87.5	80.6	61.3	81.0	75.1
	SOTR [16]	ICCV21	50.7	70.4	59.0	43.5	65.1	50.3	68.2	86.9	79.3	61.6	78.4	73.0
	Mask Transfomer [24]	CVPR22	48.7	71.0	56.3	40.7	64.5	47.2	67.5	87.6	80.4	57.8	78.9	70.3
	SparseInst [8]	CVPR22	51.3	71.9	58.9	43.1	65.1	48.5	65.0	85.0	75.7	62.8	81.3	75.3
	Mask2Former [7]	CVPR22	51.5	67.3	57.6	44.1	62.4	49.4	68.3	85.1	76.7	66.6	79.3	75.1
DSIS	CalibNet (Ours)	-	58.0	75.8	65.6	50.7	70.4	57.3	69.3	87.8	81.6	72.1	86.6	82.9

Table 1. Quantitative comparisons with 18 task-related methods for RGB-D SIS.

enhance the supervision of salient regions, which can be formulated as

$$\mathcal{L}_{bin} = \sum_{r \in \{C_2, T_3\}} \lambda_r \mathcal{L}_{bce}(\mathcal{P}_r, \mathcal{R}_o) + \sum_{d \in \{D_2, D_3\}} \lambda_d \mathcal{L}_{bce}(\mathcal{P}_d, \mathcal{R}_o), \quad (8)$$

where \mathcal{L}_{bce} is the binary cross-entropy loss, \mathcal{R}_o denotes the region-level ground truth derived from the instance-level label. \mathcal{P}_r and \mathcal{P}_d denote the region-level predictions that are generated from the RGB and depth feature maps after the encoder by adding a 1×1 convolution followed by a sigmoid function. The corresponding coefficients λ_r and λ_d are set to 0.6 and 0.4 respectively. Besides, λ_c , λ_{mask} , λ_{obj} , and λ_{bin} are empirically set to 2, 1, 1, and 1 respectively to balance the total loss function.

4. Experiments

4.1. Datasets

Existing Datasets. As a novel challenge, the available labels can be obtained from the instance-level annotations of RGB-D SOD datasets, including COME15K [54] and SIP [12]. To be specific, the COME15K dataset consists of 8,025 images with instance-level labels for training. For testing, it includes two test sets of different difficulty levels: COME15K-N with 4,600 normal samples and COME15K-D with 3,000 difficult samples. Before, Fan *et al.* [12] released an RGB-D SOD dataset with instance-level annotations, termed SIP, which embraces 929 high-resolution images for testing. In this paper, we use the instance-level training set of COME15K to train our CalibNet and evaluate the prediction results on the test sets of all datasets.

Proposed DSIS. To enrich and comprehensively evaluate the performance of RGB-D SIS methods, we build a

new exclusive RGB-D SIS dataset, called DSIS. DSIS consists of 1,940 samples with high-quality instance-level labels and corresponding depth maps for testing. To better identify salient instances from salient regions, we carefully collect about 2,500 image sources from existing RGB-D SOD datasets, including DUT-RGBD [41], NJUD [23], NLPR [40], and STERE [36]. Subsequently, five annotators manually annotate pixel-level salient instance labels based on the existing region-level labels. After that, we adopt the majority voting scheme to retain consensus labels while discarding ambiguous images. We gather a total of 1,940 images accompanied by bounding boxes, salient objects, and salient instance annotations. Compared to COME15K, the proposed DSIS guarantees consistency of region-level labels and instance-level labels, while some salient instance labels of COME15K are not in the salient regions. Staying ahead of SIP, our dataset has a greater variety of scenarios with multiple categories of instances. Further details of DSIS are available in the [supplementary material](#).

4.2. Evaluation Metrics

In accordance with previous SIS methods [39, 51], we also adopt the COCO-like evaluation metrics to evaluate RGB-D SIS models. The AP (average precision) score reflects the comprehensive performance of the tested method. AP₅₀ and AP₇₀ evaluate the predictions of salient instances more meticulously under specific mask IoU thresholds.

4.3. Implementation Details

We implement CalibNet based on Detectron2 [50] and train and test it on an RTX 3090 GPU with a batch size of 4. In the training stage, all models are trained for 50 epochs using the AdamW optimizer [34] with an initial learning rate of $2.5e-5$ and a weight decay of 0.0001. The learning rate is divided by 10 at the 35th and 45th epochs respectively. Un-

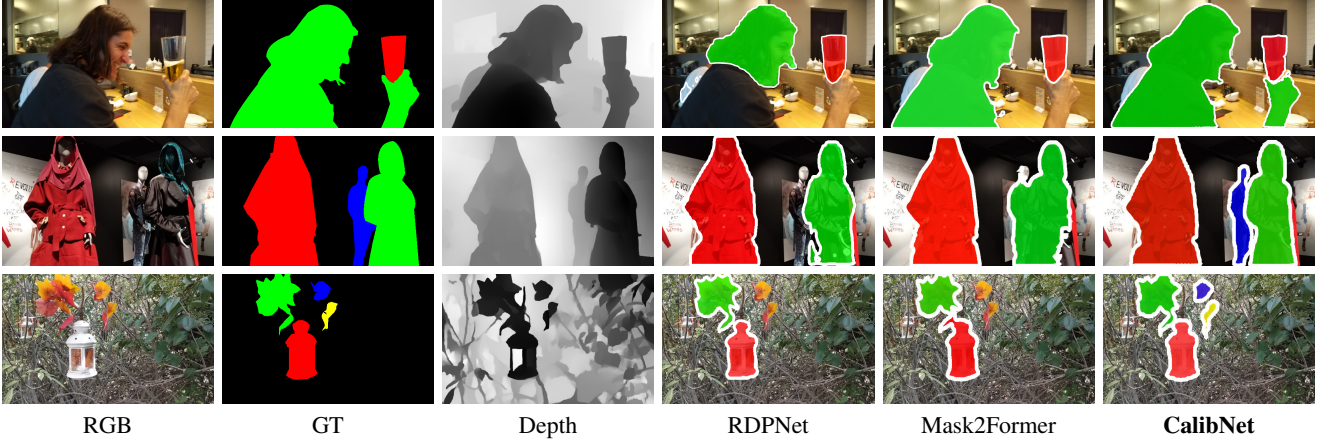


Figure 6. Visual comparison of representative models.

Method	COME15K-N [54]			COME15K-D [54]			Params	FPS
	AP	AP ₅₀	AP ₇₀	AP	AP ₅₀	AP ₇₀		
OSFormer*	50.9	71.0	58.6	43.3	65.2	50.2	78.9M	28.1
Mask2Former*	55.9	72.7	62.4	48.3	66.9	54.1	68.3M	28.0
QueryInst*	51.5	73.4	61.4	44.6	67.7	52.8	199.8M	16.9
CalibNet (Ours)	58.0	75.8	65.6	50.7	70.4	57.3	78.9M	35.9

Table 2. Performance comparison with state-of-the-art instance-level models after fusing depth modality.

less specially mentioned, we use the ResNet-50 [19] with the pre-trained weights on ImageNet [10] as the CNN backbone. All other layers are randomly initialized. The input RGB and depth images are resized as the length of the shorter side is 320 and the longer side is at most 480 according to the original aspect ratio. For data augmentation, we adopt random flipping and scale jitter. Note that, the default number of kernels N is set to 50, and the number of transformer layers in both RGB and depth encoders is 3.

4.4. Comparison with State-of-the-art Models

To the best of our knowledge, CalibNet is the first model for RGB-D SIS. For a comprehensive comparison, we bring 18 well-known task-related models: S4Net [13], RDPNet [51], and OQTR [39] from SIS; OSFormer [38] from camouflaged instance segmentation (CIS); Mask R-CNN [18], MS R-CNN [20], Cascade R-CNN [2], CenterMask [25], HTC [6], YOLACT [1], BlendMask [4], CondInst [43], SOLOv2 [47], QueryInst [14], SOTR [16], Mask Transfiner [24], SparseInst [8], and Mask2Former [7] from generic instance segmentation (GIS). For a further in-depth comparison, we select the top three above-mentioned models and enhance them with fused depth modality to directly compare with our model on the RGB-D SIS task. Notably, we uniformly use the official code to train all models on the COME15K training set and evaluate them on the test sets of COME15K, SIP, and our DSIS. Additionally, all models are based on the ResNet-50 [19] backbone with the

ImageNet [10] pre-trained weights.

Quantitative Comparison. The prediction results of all compared models are shown in Table 1. Our CalibNet consistently outperforms all competitors by a large margin across all three datasets, *e.g.*, 5.0% AP boost on the COME15K-N test set. Even on the challenging COME15K-D test set, CalibNet still reaches a 50.7% AP score and a 70.4% AP₅₀ score. It demonstrates the robustness of our method on various complex scenes. For further comparison, we pick the top three competitive models and retrain them by fusing the depth modal to their frameworks (*i.e.*, OSFormer*, Mask2Former*, and QueryInst* in Table 2). For each model, we add a parallel backbone to extract multi-scale depth features and perform multi-level fusion in the encoder. As shown in Table 2, Mask2Former* has a 4.4% AP improvement on the COME15K-N test set after merging depth data, while the performance of OSFormer* is even slightly lower than using the RGB modality only. Overall, our model still achieves superior performance to other models that have added depth information. It illustrates the efficient exploitation and integration of the depth modality by the proposed DIK and WSF modules. Under the multi-modal architecture, our model is also able to achieve a real-time inference speed of 35.9 *fps*. This result also proves that the depth modality can contribute to improved predictions of instance-level saliency detection, which is in agreement with the conclusion obtained in [11].

Qualitative Comparison. We further intuitively display typical visualization results comparing CalibNet with 2 representative methods in Fig. 6. It can be observed that our method segments salient instances more precisely in various scenes, regardless of the quality of the depth map. Compared to the visualizations of RDPNet and Mask2former, CalibNet can accurately capture instance edges and produce more intact masks no matter in the case of multi-objects or occlusions, which is also attributed to depth information calibration and enhancement. More visualization re-

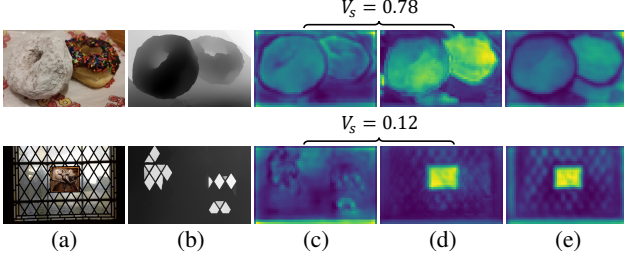


Figure 7. Visualization of attention maps in the mask branch. The top is a higher similarity case and the bottom is a lower similarity case. (a) Input image; (b) Depth map; (c) Depth feature input to DSA; (d) RGB feature input to DSA; (e) Generated mask feature.

DIK	COME15K-N			COME15K-D		
	AP	AP ₅₀	AP ₇₀	AP	AP ₅₀	AP ₇₀
Early-fusion	57.2	75.7	65.0	48.7	69.6	54.9
Later-fusion	58.0	75.8	65.6	50.7	70.4	57.3

Table 3. Ablations for the RGB and depth feature fusion in DIK.

sults can be found in the [supplementary material](#).

4.5. Ablation Study

To verify the effectiveness of the proposed model, we carry out a series of ablations on the COME15K dataset to optimize each component of CalibNet.

Modal Fusion in DIK. In the DIK module, we attempted to fuse RGB and depth features for generating kernels. Instead of using the default design that fuses two modal features after the sigmoid function (later-fusion), we also try to concatenate them first and then share the subsequent operations in DIK (early-fusion). Table 3 shows that the later-fusion style obtains higher accuracy. It can be explained that the later-fusion design can utilize the structural information and appearance features separately to cover more potential candidates when generating instance-aware kernels.

Shared Weight in WSF. For WSF module, the shared affinity weight $W_s \in \mathbb{R}^{h \times h}$ is designed as the key component to establish strong correlations between RGB and depth modalities and mine mutual information. To validate the efficiency, we try to adopt the non-local-like pattern [9, 46] in CalibNet to generate the global shared weight $W_s^g \in \mathbb{R}^{hw \times hw}$. Concretely, the RGB and depth spatial weight maps $W_r \in \mathbb{R}^{h \times w}$ and $W_d \in \mathbb{R}^{h \times w}$ are flattened to $L_r \in \mathbb{R}^{1 \times hw}$ and $L_d \in \mathbb{R}^{1 \times hw}$. Then, L_r and L_d are also operated by matrix multiplication to obtain W_s^g . For more efficient comparison, we use only the single-scale feature (T_c^3 and T_d^3) as input to the mask branch. As illustrated in Table 4, the FLOPs of the model with the non-local shared weight increase considerably, while the improvement in accuracy is limited. The FLOPs boost even to 103G when adding the low-level features (C_2, D_2) in WSF. Besides, the full-size weighting map also imposes a burden on subsequent operations, resulting in a substantial drop in the FPS

Shared Weight	AP	AP ₅₀	AP ₇₀	Params	FLOPs	FPS
Non-local ($hw \times hw$)	57.4	75.4	65.0	75.9M	64.6G	29.4
Ours ($h \times h$)	57.0	75.1	64.5	75.9M	54.0G	39.6

Table 4. Comparison of different designs for the shared affinity weight W_s in WSF on the COME15K-N test set.

DSA	COME15K-N			COME15K-D		
	AP	AP ₅₀	AP ₇₀	AP	AP ₅₀	AP ₇₀
Shared	57.0	75.6	64.2	50.3	70.4	56.7
w/o Shared	58.0	75.8	65.6	50.7	70.4	57.3

Table 5. Ablations for the effect of shared DSA in CalibNet.

Combinations	AP	AP ₅₀	AP ₇₀	Params	FLOPs	FPS
(T_c^3, T_d^3)	57.0	75.1	64.5	75.9M	54.0G	39.6
$(C_2, D_2); (T_c^3, T_d^3)$	58.0	75.8	65.6	78.9M	90.2G	35.9
$(C_2, D_2); (T_c^3, T_d^3); (T_c^4, T_d^4)$	57.3	75.6	65.0	81.9M	91.8G	35.2
$(T_c^3, T_d^3); (T_c^4, T_d^4); (T_c^5, T_d^5)$	57.1	75.4	64.7	81.9M	56.0G	35.8
$(C_2, D_2); (T_c^3, T_d^3); (T_c^4, T_d^4); (T_c^5, T_d^5)$	57.5	75.8	64.8	84.8M	92.2G	34.3

Table 6. Comparison of multiscale feature fusion in the mask branch on the COME15K-N test set.

value at the inference time. In a nutshell, the default shared affinity weight W_s makes CalibNet more flexible.

Shared Settings for DSA. CalibNet embeds the DSA module before DIK and WSF to filter out depth features for better feature consistency. In Table 5, we compare the settings of using a shared DSA versus non-shared DSAs in the mask and kernel branches. It indicates that CalibNet with shared DSA performs relatively worse because the demand for RGB and depth feature discretization is different in the mask and kernel branches. Therefore, our framework is appropriate for using non-shared DSA modules in different branches. We also visualize the input features of RGB and depth in DSA and the corresponding similarity scores in Fig. 7. We can see that the visual difference between the two modal features is consistent with the quantified scores.

Multiscale Fusion in Mask Branch. The proposed WSF is responsible for fusing cross-modal features in the mask branch. It is also essential to integrate multiscale cross-level features from RGB and depth encoders to obtain the unified mask feature. Hence, we conduct an ablation experiment to combine different layers in the mask branch so as to evaluate the effectiveness of our model. The results of various combinations are shown in Table 6. The first two rows demonstrate the importance of low-level features. Besides, adding more transformer layers has no remarkable effect while bringing more extra parameters. Considering the trade-off between accuracy and efficiency, we finally adopt the second layer in the CNN backbone (C_2, D_2) and the third layer after the transformer (T_c^3, T_d^3) for multiscale fusion. The mask feature achieved by the mask branch is also visualized in the last column of Fig. 7.

Effectiveness of Each Component. To optimize the performance of our model, we conduct an ablation study to

DIK	WSF	DSA	AP	AP ₅₀	AP ₇₀
			55.2	74.1	62.9
✓			56.5	75.3	64.0
	✓		56.7	75.1	64.1
✓		✓	56.9	75.3	64.9
	✓	✓	57.3	75.6	64.7
✓	✓		57.5	75.6	65.1
✓	✓	✓	58.0	75.8	65.6

Table 7. Ablation studies for each component of CalibNet on the COME15K-N test set.

thoroughly validate the effectiveness of each component in CalibNet, including the dynamic interactive kernel (DIK) module, the weight-sharing fusion (WSF), and the depth similarity assessment (DSA) module. Note that, we simply use the RGB feature to obtain instance-aware kernels and the mask feature as the baseline model without using any of our proposed parts. As illustrated in the first three rows of Table 7, each component has a positive impact on the performance of CalibNet, especially the contribution of DIK and WSF. Gathering all parts, our proposed CalibNet can obtain better performance compared to other variants.

5. Conclusion

This paper presents a dual-branch cross-modal calibration model called CalibNet for the RGB-D salient instance segmentation task. The model consists of two parallel branches: the kernel branch efficiently combines RGB and depth features to generate instance-aware kernels using the dynamic interactive kernel (DIK) module, while the mask branch calibrates and integrates multiscale cross-modal feature maps with the weight-sharing fusion (WSF) module to produce a mask feature. A depth similarity assessment (DSA) module is also included to suppress noisy depth information. The experiments conducted demonstrate the benefits of depth information on SIS performance and the superiority of CalibNet. Additionally, the authors have contributed a new RGB-D SIS dataset, DSIS, for the comprehensive evaluation of relevant models. This task holds great potential for enhancing other multi-modal detection tasks.

References

- [1] Daniel Bolya, Chong Zhou, Fanyi Xiao, and Yong Jae Lee. Yolact: Real-time instance segmentation. In *IEEE ICCV*, pages 9157–9166, 2019. 6, 7
- [2] Zhaowei Cai and Nuno Vasconcelos. Cascade r-cnn: high quality object detection and instance segmentation. *IEEE TPAMI*, 43(5):1483–1498, 2019. 6, 7
- [3] Nicolas Carion, Francisco Massa, Gabriel Synnaeve, Nicolas Usunier, Alexander Kirillov, and Sergey Zagoruyko. End-to-end object detection with transformers. In *ECCV*, pages 213–229, 2020. 2, 4, 5
- [4] Hao Chen, Kunyang Sun, Zhi Tian, Chunhua Shen, Yongming Huang, and Youliang Yan. Blendmask: Top-down meets bottom-up for instance segmentation. In *IEEE CVPR*, pages 8573–8581, 2020. 6, 7
- [5] Kai Chen, Lanqing Hong, Hang Xu, Zhenguo Li, and Dit-Yan Yeung. Multisiam: Self-supervised multi-instance siamese representation learning for autonomous driving. In *IEEE ICCV*, pages 7546–7554, 2021. 1
- [6] Kai Chen, Jiangmiao Pang, Jiaqi Wang, Yu Xiong, Xiao-xiao Li, Shuyang Sun, Wansen Feng, Ziwei Liu, Jianping Shi, Wanli Ouyang, et al. Hybrid task cascade for instance segmentation. In *IEEE CVPR*, pages 4974–4983, 2019. 6, 7
- [7] Bowen Cheng, Ishan Misra, Alexander G Schwing, Alexander Kirillov, and Rohit Girdhar. Masked-attention mask transformer for universal image segmentation. In *IEEE CVPR*, pages 1290–1299, 2022. 1, 4, 6, 7, 15, 16
- [8] Tianheng Cheng, Xinggang Wang, Shaoyu Chen, Wenqiang Zhang, Qian Zhang, Chang Huang, Zhaoxiang Zhang, and Wenyu Liu. Sparse instance activation for real-time instance segmentation. In *IEEE CVPR*, pages 4433–4442, 2022. 2, 5, 6, 7, 11
- [9] Runmin Cong, Qinwei Lin, Chen Zhang, Chongyi Li, Xiaochun Cao, Qingming Huang, and Yao Zhao. Cir-net: Cross-modality interaction and refinement for rgb-d salient object detection. *IEEE TIP*, 31:6800–6815, 2022. 5, 8
- [10] Jia Deng, Wei Dong, Richard Socher, Li-Jia Li, Kai Li, and Li Fei-Fei. Imagenet: A large-scale hierarchical image database. In *IEEE CVPR*, pages 248–255, 2009. 7, 11
- [11] Karthik Desingh, K Madhava Krishna, Deepu Rajan, and CV Jawahar. Depth really matters: Improving visual salient region detection with depth. In *BMVC*, pages 1–11, 2013. 7
- [12] Deng-Ping Fan, Zheng Lin, Zhao Zhang, Menglong Zhu, and Ming-Ming Cheng. Rethinking rgb-d salient object detection: Models, data sets, and large-scale benchmarks. *IEEE TNNLS*, 32(5):2075–2089, 2020. 2, 6, 12, 14
- [13] Ruochen Fan, Ming-Ming Cheng, Qibin Hou, Tai-Jiang Mu, Jingdong Wang, and Shi-Min Hu. S4net: Single stage salient-instance segmentation. In *IEEE CVPR*, pages 6103–6112, 2019. 1, 2, 6, 7
- [14] Yuxin Fang, Shusheng Yang, Xinggang Wang, Yu Li, Chen Fang, Ying Shan, Bin Feng, and Wenyu Liu. Instances as queries. In *IEEE CVPR*, pages 6910–6919, 2021. 6, 7
- [15] Jia-Chang Feng, Fa-Ting Hong, and Wei-Shi Zheng. Mist: Multiple instance self-training framework for video anomaly detection. In *IEEE CVPR*, pages 14009–14018, 2021. 1
- [16] Ruohao Guo, Dantong Niu, Liao Qu, and Zhenbo Li. Sotr: Segmenting objects with transformers. In *IEEE ICCV*, pages 7157–7166, 2021. 6, 7
- [17] Saurabh Gupta, Ross Girshick, Pablo Arbeláez, and Jitendra Malik. Learning rich features from rgb-d images for object detection and segmentation. In *ECCV*, pages 345–360, 2014. 3
- [18] Kaiming He, Georgia Gkioxari, Piotr Dollár, and Ross Girshick. Mask r-cnn. In *IEEE ICCV*, pages 2961–2969, 2017. 1, 2, 6, 7
- [19] Kaiming He, Xiangyu Zhang, Shaoqing Ren, and Jian Sun. Deep residual learning for image recognition. In *IEEE CVPR*, 2016. 3, 7, 11, 12, 13

- [20] Zhaojin Huang, Lichao Huang, Yongchao Gong, Chang Huang, and Xinggang Wang. Mask scoring r-cnn. In *IEEE CVPR*, pages 6409–6418, 2019. 6, 7
- [21] Wei Ji, Jingjing Li, Shuang Yu, Miao Zhang, Yongri Piao, Shunyu Yao, Qi Bi, Kai Ma, Yefeng Zheng, Huchuan Lu, et al. Calibrated rgb-d salient object detection. In *IEEE CVPR*, pages 9471–9481, 2021. 1
- [22] Yueming Jin, Yang Yu, Cheng Chen, Zixu Zhao, Pheng-Ann Heng, and Danail Stoyanov. Exploring intra-and inter-video relation for surgical semantic scene segmentation. *IEEE TMI*, 2022. 1
- [23] Ran Ju, Yang Liu, Tongwei Ren, Ling Ge, and Gangshan Wu. Depth-aware salient object detection using anisotropic center-surround difference. *Signal Processing: Image Communication*, 38:115–126, 2015. 6, 12
- [24] Lei Ke, Martin Danelljan, Xia Li, Yu-Wing Tai, Chi-Keung Tang, and Fisher Yu. Mask transfiner for high-quality instance segmentation. In *IEEE CVPR*, pages 4412–4421, 2022. 6, 7
- [25] Youngwan Lee and Jongyoul Park. Centermask: Real-time anchor-free instance segmentation. In *IEEE CVPR*, pages 13906–13915, 2020. 6, 7
- [26] Guanbin Li, Yuan Xie, Liang Lin, and Yizhou Yu. Instance-level salient object segmentation. In *IEEE CVPR*, pages 2386–2395, 2017. 2
- [27] Yin Li, Xiaodi Hou, Christof Koch, James M Rehg, and Alan L Yuille. The secrets of salient object segmentation. In *IEEE CVPR*, pages 280–287, 2014. 12
- [28] Tsung-Yi Lin, Priya Goyal, Ross Girshick, Kaiming He, and Piotr Dollár. Focal loss for dense object detection. In *IEEE ICCV*, pages 2980–2988, 2017. 5
- [29] Nian Liu, Ni Zhang, Ling Shao, and Junwei Han. Learning selective mutual attention and contrast for rgb-d saliency detection. *IEEE TPAMI*, 44(12):9026–9042, 2021. 5
- [30] Nian Liu, Ni Zhang, Kaiyuan Wan, Ling Shao, and Junwei Han. Visual saliency transformer. In *IEEE ICCV*, pages 4722–4732, 2021. 1
- [31] Nian Liu, Wangbo Zhao, Ling Shao, and Junwei Han. Scg: Saliency and contour guided salient instance segmentation. *IEEE TIP*, 30:5862–5874, 2021. 3
- [32] Rosanne Liu, Joel Lehman, Piero Molino, Felipe Petroski Such, Eric Frank, Alex Sergeev, and Jason Yosinski. An intriguing failing of convolutional neural networks and the coordconv solution. In *NeurIPS*, 2018. 4
- [33] Ze Liu, Yutong Lin, Yue Cao, Han Hu, Yixuan Wei, Zheng Zhang, Stephen Lin, and Baining Guo. Swin transformer: Hierarchical vision transformer using shifted windows. In *IEEE ICCV*, pages 10012–10022, 2021. 11, 12
- [34] Ilya Loshchilov and Frank Hutter. Decoupled weight decay regularization. In *ICLR*, 2019. 6
- [35] Fausto Milletari, Nassir Navab, and Seyed-Ahmad Ahmadi. V-net: Fully convolutional neural networks for volumetric medical image segmentation. In *3DV*, pages 565–571, 2016. 5
- [36] Yuzhen Niu, Yujie Geng, Xueqing Li, and Feng Liu. Leveraging stereopsis for saliency analysis. In *IEEE CVPR*, pages 454–461, 2012. 6, 12
- [37] Nobuyuki Otsu. A threshold selection method from gray-level histograms. *IEEE Trans. Syst. Man Cybern.*, 9(1):62–66, 1979. 13
- [38] Jialun Pei, Tianyang Cheng, Deng-Ping Fan, He Tang, Chuanbo Chen, and Luc Van Gool. Osformer: One-stage camouflaged instance segmentation with transformers. In *ECCV*, pages 19–37, 2022. 6, 7
- [39] Jialun Pei, Tianyang Cheng, He Tang, and Chuanbo Chen. Transformer-based efficient salient instance segmentation networks with orientative query. *IEEE TMM*, 2022. 3, 6, 7
- [40] Houwen Peng, Bing Li, Weihua Xiong, Weiming Hu, and Rongrong Ji. Rgb-d salient object detection: A benchmark and algorithms. In *ECCV*, pages 92–109, 2014. 6, 12
- [41] Yongri Piao, Wei Ji, Jingjing Li, Miao Zhang, and Huchuan Lu. Depth-induced multi-scale recurrent attention network for saliency detection. In *IEEE ICCV*, pages 7254–7263, 2019. 6, 12
- [42] Xin Tian, Ke Xu, Xin Yang, Baocai Yin, and Rynson WH Lau. Learning to detect instance-level salient objects using complementary image labels. *IJCV*, 130(3):729–746, 2022. 3
- [43] Zhi Tian, Chunhua Shen, and Hao Chen. Conditional convolutions for instance segmentation. In *ECCV*, pages 282–298, 2020. 6, 7
- [44] Jonas Uhrig, Marius Cordts, Uwe Franke, and Thomas Brox. Pixel-level encoding and depth layering for instance-level semantic labeling. In *GCPR*, pages 14–25, 2016. 3
- [45] Wenhai Wang, Enze Xie, Xiang Li, Deng-Ping Fan, Kaitao Song, Ding Liang, Tong Lu, Ping Luo, and Ling Shao. Pvt v2: Improved baselines with pyramid vision transformer. *CVMJ*, 8(3):415–424, 2022. 11, 12
- [46] Xiaolong Wang, Ross Girshick, Abhinav Gupta, and Kaiming He. Non-local neural networks. In *IEEE CVPR*, pages 7794–7803, 2018. 5, 8
- [47] Xinlong Wang, Rufeng Zhang, Chunhua Shen, Tao Kong, and Lei Li. Solo: A simple framework for instance segmentation. *IEEE TPAMI*, 2021. 1, 2, 6, 7
- [48] Hongfa Wen, Chenggang Yan, Xiaofei Zhou, Runmin Cong, Yaoqi Sun, Bolun Zheng, Jiyong Zhang, Yongjun Bao, and Guiguang Ding. Dynamic selective network for rgb-d salient object detection. *IEEE TIP*, 30:9179–9192, 2021. 1
- [49] Sanghyun Woo, Jongchan Park, Joon-Young Lee, and In So Kweon. Cbam: Convolutional block attention module. In *ECCV*, pages 3–19, 2018. 4
- [50] Yuxin Wu, Alexander Kirillov, Francisco Massa, Wan-Yen Lo, and Ross Girshick. Detectron2. <https://github.com/facebookresearch/detectron2>, 2019. 6
- [51] Yu-Huan Wu, Yun Liu, Le Zhang, Wang Gao, and Ming-Ming Cheng. Regularized densely-connected pyramid network for salient instance segmentation. *IEEE TIP*, 30:3897–3907, 2021. 3, 6, 7
- [52] Yu Xiang, Christopher Xie, Arsalan Mousavian, and Dieter Fox. Learning rgb-d feature embeddings for unseen object instance segmentation. In *Conference on Robot Learning*, pages 461–470, 2021. 3

- [53] Zhengtian Xu, Shu Liu, Jianping Shi, and Cewu Lu. Outdoor rgbd instance segmentation with residual regretting learning. *IEEE TIP*, 29:5301–5309, 2020. **2, 3**
- [54] Jing Zhang, Deng-Ping Fan, Yuchao Dai, Xin Yu, Yiran Zhong, Nick Barnes, and Ling Shao. Rgb-d saliency detection via cascaded mutual information minimization. In *IEEE ICCV*, pages 4338–4347, 2021. **2, 6, 7, 11, 12, 14**
- [55] Tao Zhou, Deng-Ping Fan, Ming-Ming Cheng, Jianbing Shen, and Ling Shao. Rgb-d salient object detection: A survey. *CVMJ*, 7(1):37–69, 2021. **1**
- [56] Tao Zhou, Huazhu Fu, Geng Chen, Yi Zhou, Deng-Ping Fan, and Ling Shao. Specificity-preserving rgb-d saliency detection. In *IEEE ICCV*, pages 4681–4691, 2021. **1**
- [57] Xizhou Zhu, Weijie Su, Lewei Lu, Bin Li, Xiaogang Wang, and Jifeng Dai. Deformable detr: Deformable transformers for end-to-end object detection. In *ICLR*, 2020. **3**

Appendix

We summarize the supplementary material from the following aspects:

Ablation Studies. We collate more detailed ablation studies to improve the performance of our model, including the number of instance-aware kernels (Table 8), the number of deformable transformer layers (Table 9), coefficients of the total loss function (Table 10), and performance of CalibNet with different backbones (Table 11).

DSIS Dataset. More visual annotations and statistics in DSIS are presented in Fig. 8 and Fig. 9. Datasets for the RGB-D SIS task are also analyzed and discussed (refer to Fig. 10, Fig. 11, and Fig. 12).

Limitations. We display and analyze some typical failure cases to guide future RGB-D SIS works (Fig. 13).

Additional Qualitative Results. Additional visual results of our CalibNet in all test sets are shown in Fig. 14.

6. Ablation Studies

6.1. Number of Kernels

The appropriate number of instance-aware kernels can adequately locate potentially salient instances and balance the accuracy and efficiency of the proposed CalibNet. To investigate the effect of the number of kernels, we perform an ablation experiment with different numbers of kernels N (10, 20, 50, and 100). As shown in Table 8, the performance of CalibNet improves consistently with the increase in the number of kernels. When N is greater than 50, the improvement in accuracy becomes marginal, and even the AP value drops slightly on the COME15K-D test set. Trading off the accuracy and efficiency of our model, the number of instance-aware kernels N in CalibNet is set to 50.

6.2. Number of Transformer Layers

The integration of deformable transformer layers into both RGB and depth encoders in CalibNet is aimed at en-

N	COME15K-N			COME15K-D			Params	GFLOPs
	AP	AP ₅₀	AP ₇₀	AP	AP ₅₀	AP ₇₀		
10	56.5	75.0	64.0	48.5	69.2	54.3	78.7M	89.5
20	57.2	75.2	64.6	50.0	70.3	56.1	78.8M	89.7
50	58.0	75.8	65.6	50.7	70.4	57.3	78.9M	90.2
100	58.1	76.3	65.6	50.3	70.9	57.2	79.2M	91.2

Table 8. Ablations for different numbers of instance-aware kernels.

Number		COME15K-N			COME15K-D			Params
RGB	Depth	AP	AP ₅₀	AP ₇₀	AP	AP ₅₀	AP ₇₀	
3	0	57.2	75.4	64.9	49.6	70.5	56.4	76.7M
3	1	57.1	75.7	65.0	49.0	69.9	55.3	77.4M
3	3	58.0	75.8	65.6	50.7	70.4	57.3	78.9M
6	1	55.4	74.6	63.2	47.2	69.0	52.9	79.6M
6	3	58.2	76.3	65.8	50.6	70.9	57.0	81.1M
6	6	58.0	76.1	65.3	50.4	70.9	56.8	83.3M

Table 9. Performance of CalibNet with different combinations of the number of transformer layers in RGB and depth encoders.

hancing the capture of global information. To optimize the performance of our model, we experimented with different combinations of the number of layers on the RGB and depth encoders. As illustrated in Table 9, the first row indicates that it is not appropriate to add transformer layers to only the RGB modality. When the number of layers in RGB and depth encoders is 3 and 3, respectively, CalibNet achieves promising results in both COME15K-N and COME15k-D test sets [54]. Although increasing the number of transformer layers in the RGB encoder to 6 leads to higher AP values on the COME15K-N test set, the additional parameters of the model could have a negative impact on the multimodal architecture. As a result, the default number of transformer layers in RGB and depth encoders is set to 3 for both modalities.

6.3. Coefficients of Total Loss Function

In the total loss function of CalibNet (see Eq.(6) in manuscript), we use four weight coefficients (λ_c , λ_{mask} , λ_{obj} , and λ_{bin}) to improve the efficiency of model training. We attempt different combinations of coefficients for location loss \mathcal{L}_c , mask loss \mathcal{L}_{mask} , objectness loss \mathcal{L}_{obj} , and auxiliary loss \mathcal{L}_{bin} in Table 10. Notably, we set the coefficient λ_{obj} of objectness loss as 1 in line with [8], and λ_{bin} is also fixed to 1. The ablation results demonstrate that the optimal performance is achieved when the value of λ_c , λ_{mask} , λ_{obj} , and λ_{bin} are set to 2, 1, 1, and 1, respectively.

6.4. Performance of Different Backbones

To exploit the potential of our model, we adopt several backbone networks with ImageNet [10] pre-trained weights to train CalibNet, including ResNet-50 [19], ResNet-101 [19], Swin-T [33], and PVTv2-B2-Li [45]. As shown in Table 11, CalibNet can achieve 58.0% AP values based on the default ResNet-50. With a stronger backbone network

Coefficients				COME15K-N			COME15K-D		
λ_c	λ_{mask}	λ_{obj}	λ_{bin}	AP	AP ₅₀	AP ₇₀	AP	AP ₅₀	AP ₇₀
1	1	1	1	56.4	75.0	64.1	48.3	69.4	54.6
2	1	1	1	58.0	75.8	65.6	50.7	70.4	57.3
5	1	1	1	55.1	74.4	63.0	47.0	68.8	53.2
5	2	1	1	57.2	75.7	64.7	49.6	70.4	56.0
10	5	1	1	55.6	75.0	63.5	48.4	70.1	54.8

Table 10. Ablations on the weight coefficients in the total loss.

Backbones	COME15K-N			COME15K-D		
	AP	AP ₅₀	AP ₇₀	AP	AP ₅₀	AP ₇₀
ResNet-50 [19]	58.0	75.8	65.6	50.7	70.4	57.3
ResNet-101 [19]	58.5	76.4	66.0	51.5	71.8	58.0
Swin-T [33]	60.0	77.9	67.5	52.6	72.9	58.6
PVTv2-B2-Li [45]	60.7	78.1	67.8	53.7	72.9	59.6

Table 11. Performance of CalibNet with different backbones.

(i.e., Swin-T), our model further reaches 60.7% AP on the COME15K-N test set. It indicates that the performance of our model still has considerable scalability.

7. DSIS Dataset

7.1. Dataset Statistics

In order to create a robust RGB-D SIS benchmark and thoroughly evaluate the generalization performance of task-specific models, we released a new RGB-D SIS dataset, namely DSIS. To ensure a high degree of consistency in the instance-level labels and salient regions, we collected data sources with region-level annotations and depth maps directly from the existing RGB-D SOD datasets, including NJUD [23], DUT-RGBD [41], STERE [36], and NLPR [40]. Following a rigorous data cleaning process (as described in Section 4.1 in the manuscript), we retained a total of 1,940 samples for instance-level annotation, and the final distribution of data sources is provided on the left of Fig. 8. All images with instance-level ground truth are used for the test set to enrich the evaluation diversity. As shown in the right of Fig. 8, we also gathered the distribution of the number of salient instances in each image.

Based on the existing SOD ground truth, we performed fine-grained instance-level annotations, resulting in a more comprehensive evaluation of RGB-D SIS models. Examples of the typical annotated instances are exhibited in Fig. 9. We can see that our DSIS dataset contains a wide variety of scenarios and a diversity of instance appearances, including complex backgrounds, illumination changes, low contrast, high edge complexity, and so on. In various scenarios, we have provided elaborate labels of salient instances, e.g., low-contrast airplanes, snakes under illumination changes, and vimineous bow and arrow in the column of the intricate edge. The diversity of salient instances will bring a more comprehensive evaluation of RGB-D saliency detection models. By releasing DSIS, we hope to facilitate fur-

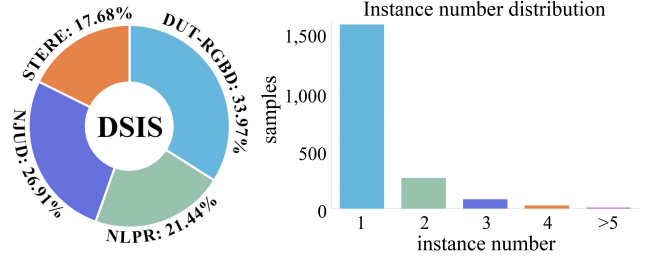


Figure 8. Distribution of the DSIS dataset. Left: Distribution of image sources collected from RGB-D SOD datasets. Right: Distribution of the number of salient instances in each sample.

ther research and development in the field of RGB-D SIS.

7.2. Dataset Analysis and Comparison

Center Bias. The distribution of instance centers is a crucial metric that can reveal whether a dataset suffers from center bias, i.e., whether salient instances tend to be biased toward the center of the scene. A more dispersed distribution of instance centers indicates greater instance diversity in the dataset. Fig. 10 demonstrates that all RGB-D SIS datasets suffer from less center bias in different degrees. Specifically, the instance centers in the COME15K-N and COME15K-D test sets [54] tend to be biased in the cross direction, while the instance distribution of the SIP dataset [12] is concentrated mainly in the lower center. In comparison, the instance centers in our DSIS dataset are diffused more uniformly in all directions.

Instance Size Distribution. The distribution of instance sizes is also an important factor in evaluating the quality of a dataset since it provides insights into the variation and diversity of instances present in the images. The general metric for measuring instance sizes is the ratio of instance pixels to the total image pixels [27]. As depicted in Fig. 11 (a), we observe that the distribution of instance sizes in the DSIS and COME15K datasets cover a wide range, while the SIP dataset displays less variation in instance sizes. Notably, our DSIS dataset exhibits a higher proportion of medium-sized instances. On the other hand, the COME15K dataset primarily comprises smaller-sized instances.

Objects/Instances Consistency. As is well known, the SIS task is defined as the further partitioning of salient instances within salient regions. To ensure the accuracy of salient instance annotations, it is crucial to label them within the salient object-level ground truth. To verify the consistency between the two levels of labeling, we binarized the salient instance labels and calculated the average Intersection over Union (IoU) between the binarized instance labels and salient object labels. The matching curves in Fig. 11 (b) illustrate that object- and instance-level ground truth in both SIP and DSIS are absolutely aligned, while the average IoU values in the two COME15K test sets have decreased

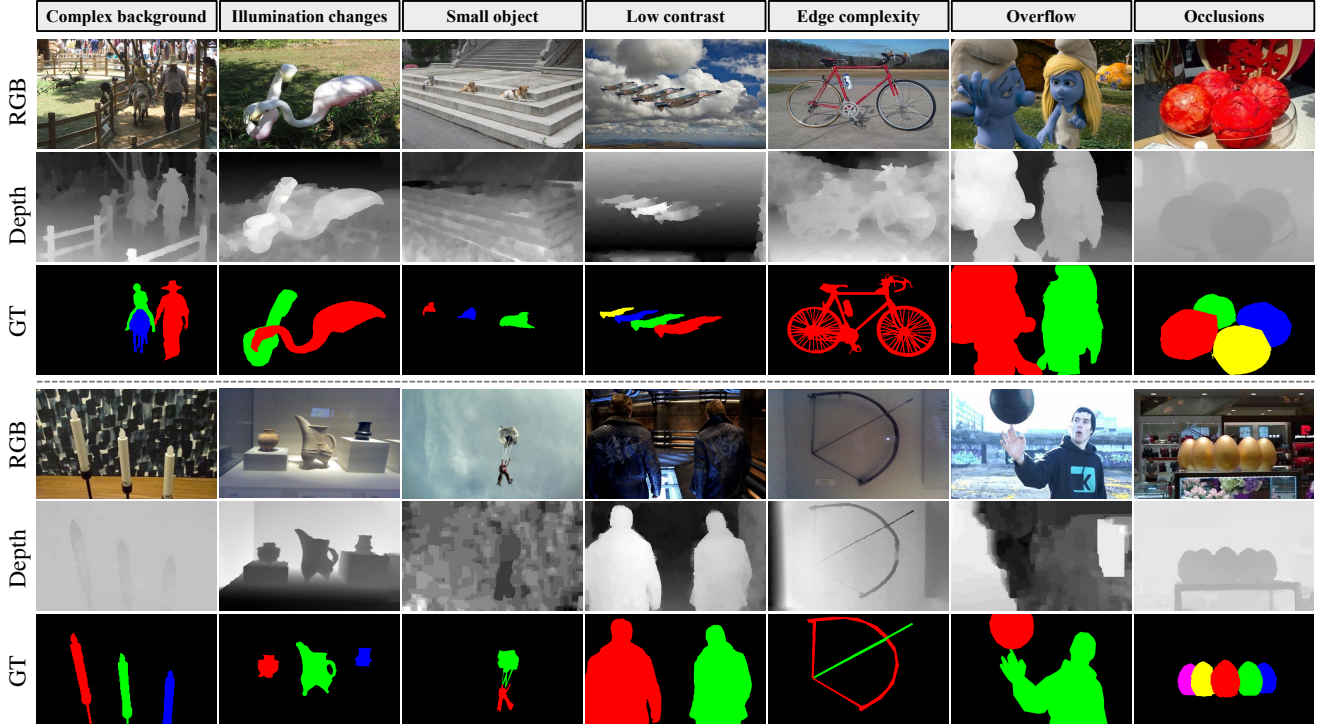


Figure 9. Example of a diverse annotation of the proposed DSIS dataset.

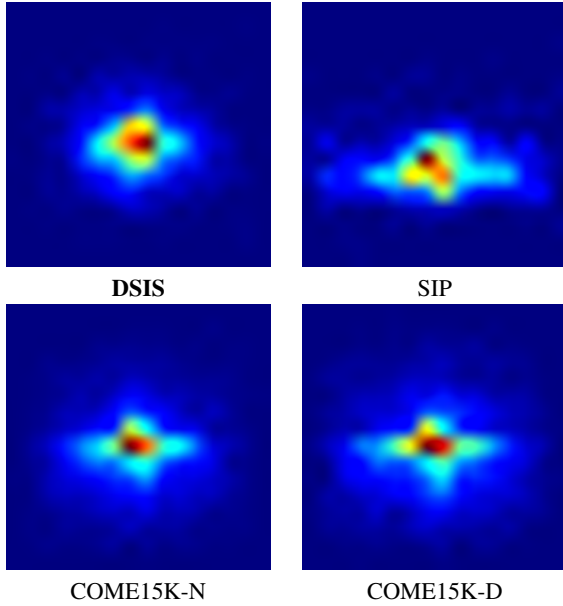


Figure 10. Instance center bias of RGB-D SIS datasets.

to varying degrees. This implies that the salient instance labels in COME15K are not completely salient, leading to a decrease in the quality of instance labels. Fig. 12 provides typical samples that visually illustrate the inconsistency between the object- and instance-level ground truth in COME15K.

Depth/Saliency Consistency. As an RGB-D instance-level saliency detection task, the consistency between the structural information provided by the depth maps and the salient object labels can assess the difficulty of the RGB-D datasets. In this regard, we make a simple binarization of the depth maps for a more direct consistency comparison with the salient object labels. Specifically, we first adopt the OTSU algorithm [37] to binarize the depth maps. Then, the foreground and background area is reversed to keep the indexes of salient and spatially closer objects consistent. Fig. 11 (c) shows the matching curves between the binarized depth maps and salient object labels in all datasets. It is interesting to note that the matching degree between the two modalities is below 50% in all datasets, which also illustrates that proximity to the camera does not necessarily indicate saliency. From this perspective, it is essential to calibrate and purify the depth information in the RGB-D segmentation model. The consistency between the depth map and saliency labels in our DSIS dataset is the lowest compared to other datasets, which poses a greater challenge for cross-modal models. We expect that our DSIS will encourage the development of more efficient RGB-D SIS models that can better filter and integrate cross-modal information.

8. Limitations

We display several typical failure cases generated by the proposed CalibNet with ResNet-50 [19] on the COME15K

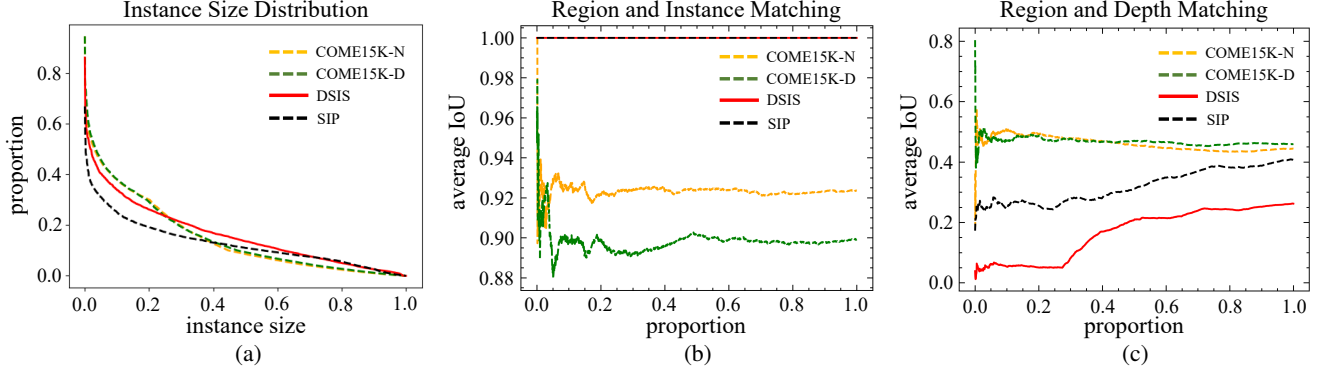


Figure 11. Comparison between the proposed DSIS and existing datasets for RGB-D SIS task. (a) Distribution of instance sizes in all test sets; (b) Comparison of the consistency between salient object-level ground truth and binarized instance-level ground truth; (c) Consistency of the salient object ground truth with the binarized depth map.

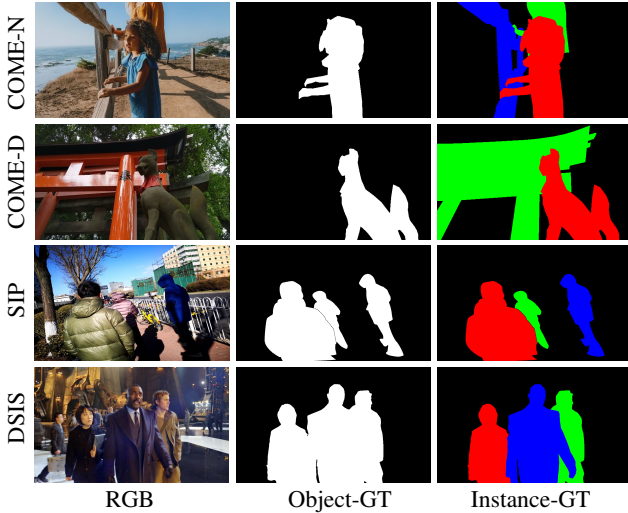


Figure 12. Comparison of the consistency between salient object-level ground truth and instance-level ground truth in RGB-D saliency datasets.

test set in Fig. 13. The first row indicates that CalibNet has a tendency to overlook certain smaller targets when presented with both small and large targets simultaneously. This could be attributed to the negative feedback given by the depth map, resulting in the generated kernels disregarding the smaller instance embeddings. The middle sample illustrates that low contrast and complex object edges can lead to suboptimal segmentation results. This problem can be mitigated by introducing edge priors or embedding the operation of highlight edge cues. Additionally, if the background of the scene is overly cluttered (see the bottom sample), CalibNet has the potential to over-segment salient instances. This issue drives us to further improved to handle increasingly complex scenarios, including the ability to better understand and differentiate salient instances from the background in cluttered scenes.

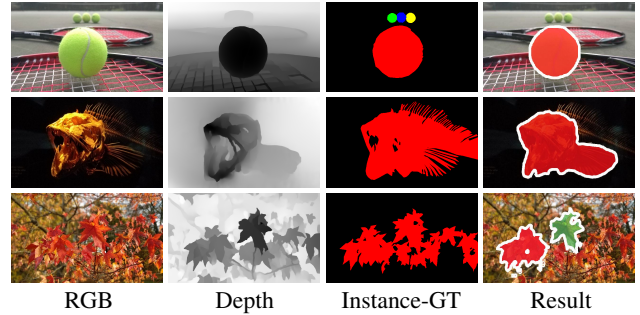


Figure 13. Typical failure results produced by CalibNet.

9. Additional Qualitative Results

We exhibit more visual results of our proposed CalibNet evaluated on four RGB-D SIS test sets, COME15K-N, COME15K-D [54], DSIS, and SIP test sets [12]. As shown in Fig. 14, the visualizations demonstrate our CalibNet is capable of accurately identifying and segmenting the most visually salient instances in a variety of scenes, while suppressing background clutter and other irrelevant targets. For instance, in the top image of Fig. 14, which contains two girls and various recreational facilities, CalibNet can precisely discriminate them while suppressing the toy vehicle in front of the image. Even in the presence of complex backgrounds with cluttered attributes, such as the third and fourth rows in Fig. 14, the proposed model is still able to accurately detect salient instances. In the face of changing illumination, especially when the goals have smaller sizes (the fifth and seventh rows), our method can still handle it. More importantly, as an instance-level RGB-D model, CalibNet is shown to be effective in handling a range of challenging scenarios even though the structural information of the depth map has a strong misalignment with salient regions (the first, sixth, and seventh rows). It demonstrates the efficiency of our WSF and DSA module in the calibration of cross-modal features. Compared to other

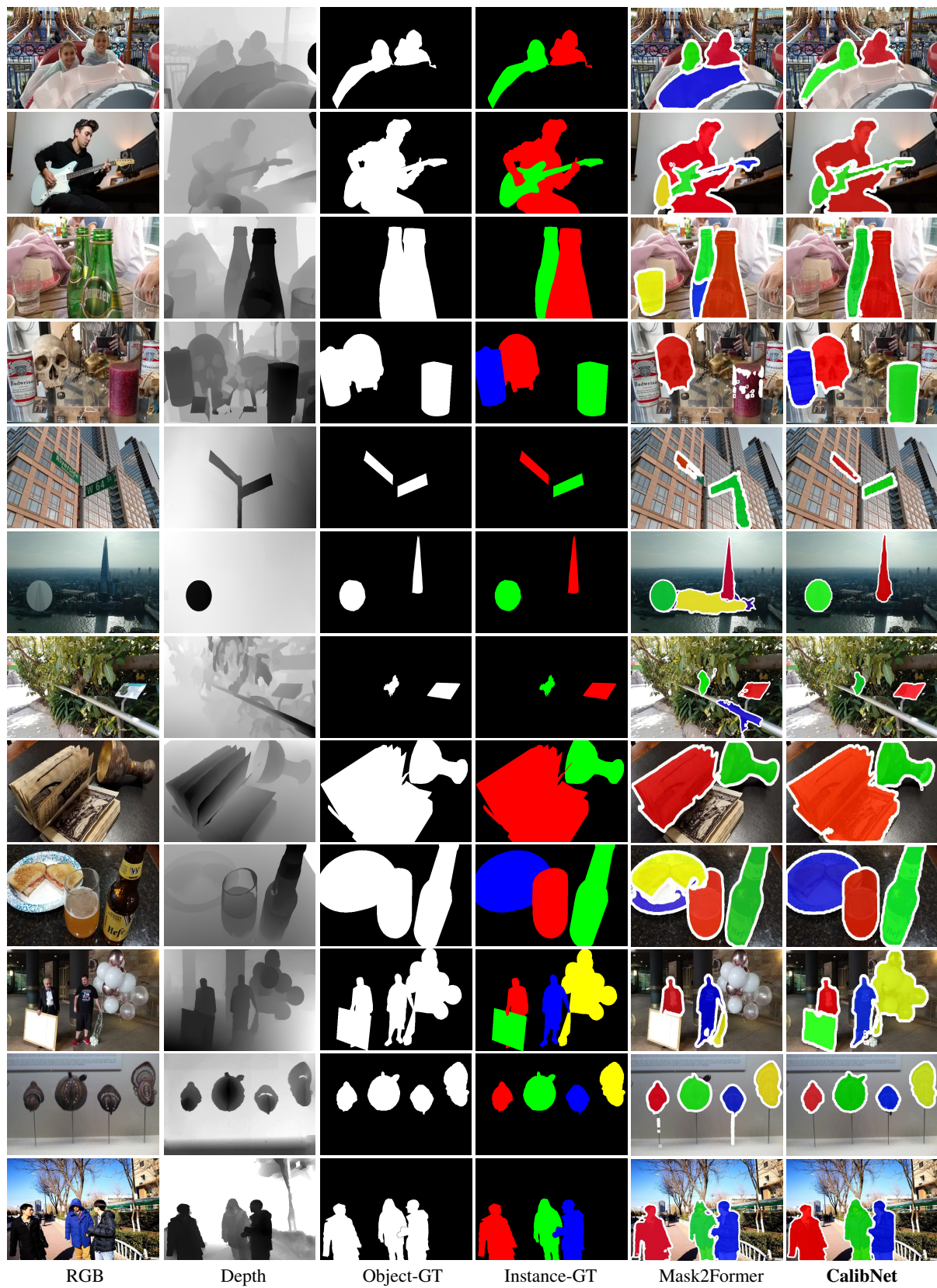


Figure 14. Additional visualizations of CalibNet and Mask2Former [7] on the COME15K-N, COME15K-D, DSIS, and SIP test sets.

state-of-the-art models, like Mask2Former [7], our model provides better suppression of background noise and more robust predictions of the number of salient instances, making it a promising approach for a wide range of computer vision applications, such as tracking, autonomous driving, and scene understanding.